Journal of Asian Earth Sciences 155 (2018) 49–57

Contents lists available at ScienceDirect

Journal of Asian Earth Sciences

journal homepage: www.elsevier.com/locate/jseaes

Full length article

Hydroclimatic variability in loess δD_{wax} records from the central Chinese Loess Plateau over the past 250 ka

Zheng Wang[a,*], Zhisheng An[a,b], Zhonghui Liu[c], Xiaoke Qiang[a], Fan Zhang[b], Weiguo Liu[a,b]

[a] State Key Laboratory of Loess and Quaternary Geology, IEE, CAS, Xi'an 710075, China
[b] School of Human Settlement and Civil Engineering, Xi'an Jiaotong University, Xi'an 710049, China
[c] Department of Earth Sciences, The University of Hong Kong, Hong Kong, China

ARTICLE INFO

Keywords:
Loess δD_{wax}
Central Chinese Loess Plateau
Asian Summer Monsoon
Hydroclimatic changes

ABSTRACT

This study reports hydrogen isotopic records from the central Chinese Loess Plateau (CLP) over the past 250 ka. After eliminating the influence of ice and local temperatures, the δD_{wax} records extracted from two loess sites at Xifeng and Luochuan can be taken to represent arid/humid alternations in the hydrological environment in this marginal Asian Summer Monsoon (ASM) region; they also contain integrated information on summer precipitation patterns and the corresponding responses to these changes by predominant vegetation cover types. These arid/humid alternations show 100 ka, 40 ka and 20 ka cycles. An increase in precipitation in association with an enhanced summer monsoon has historically been taken to be the major factor driving a humid environment in the central CLP. However, hydroclimatic changes in δD_{wax} records differ for the central CLP, central China and southern China. Over a 20 ka cycle, the influence of solar insolation on hydroclimatic changes can be shown to be consistent throughout the central CLP. However, changes in the relative location of the land and sea may have caused different hydroclimatic responses between southern China and the central CLP on a glacial-interglacial scale. The hydroclimatic variability in the central CLP would suggest that an enhanced summer monsoon due to climatic warming is the key to understanding decreased drought degree in this marginal monsoonal region.

1. Introduction

Global warming caused by high levels of CO_2 emissions during the Anthropocene has become an established fact (Waters et al., 2016). Changing thermal land-sea conditions are altering atmospheric circulation patterns, monsoonal strength and any corresponding precipitation, thereby increasing the risk of natural disasters such as droughts and floods (Pachauri et al., 2014). On the Chinese Loess Plateau (CLP), a marginal region affected by the Asian Summer Monsoon (ASM), meteorological records indicate a rapid rise in temperature accompanied by a significant reduction in precipitation since the mid-1980s; further, it is apparent that climate warming has accelerated the likelihood that the CLP will experience drought (Sun and Ma, 2015). Theoretically, however, any climate warming and strengthening of the monsoon would push the rainbelt northward, and the central CLP would become gradually moist (Liu et al., 1991; An, 2000). During the warming mid-Holocene, the monsoonal rainbelt migrated northwest at least 300 km from its Last Glacial Maximum (LGM) extent (Yang et al., 2015). Thus, the impact of climate warming on regional hydroclimatic conditions varies significantly over different timescales. Because potential drought-induced decreases in vegetation coverage or food production can be fatal to fragile ecosystems and populations (Pachauri et al., 2014), understanding the multiscale hydroclimatic background is helpful for developing effective strategies to respond to global warming and drought, especially in the ASM-marginal CLP region. More than 200 million people live in this region and would benefit from this improved understanding.

The compound-specific hydrogen isotopic composition of plant wax (δD_{wax}) can record the isotopic ratio of water acquired during plant growth (Sessions et al., 1999; Liu and Yang, 2008; Sachse et al., 2012). Therefore, δD_{wax} values are considered to be a direct indicator of hydroclimatic changes (Hou et al., 2007; Wang et al., 2013; Tierney and deMenocal, 2013; Yao et al., 2015; Thomas et al., 2014, 2016). In a previous study, a 130-ka δD_{wax} record was used for the first time as a proxy aridity record for the central CLP (Liu and Huang, 2005). Here, we report on two combined loess-δD_{wax} series from Xifeng and Luochuan that span the last 250 ka and include two complete glacial-interglacial cycles. Our aims are: (1) to reconstruct δD_{wax} record and the hydroclimatic history of the central CLP, (2) to discuss the climatic and environmental effects on δD_{wax} values and the natural hydroclimatic

* Corresponding author.
E-mail address: wangz@ieecas.cn (Z. Wang).

https://doi.org/10.1016/j.jseaes.2017.11.008
Received 12 September 2017; Received in revised form 2 November 2017; Accepted 2 November 2017
Available online 04 November 2017

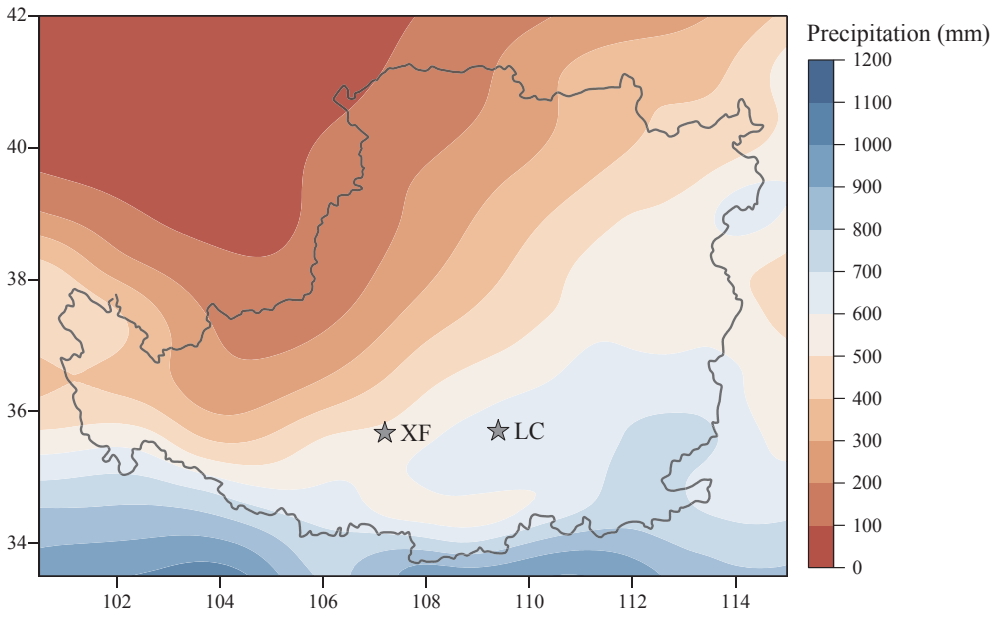

Fig. 1. Mean annual precipitation (MAP) values for the CLP. The locations of the XFJ3 and LCJ3 cores are marked in the figure. MAP data were taken from the Modern-Era Retrospective Analysis for Research and Application (MERRA).

variability in this ASM-marginal region.

2. Material and methods

2.1. Loess sequence

Samples were collected from two loess sites at Luochuan (LCJ3; above S2 layer; 35°44′34.2″N, 109°25′59.8″E) and Xifeng (XFJ3; S2-L2 layer; 35°39′58.4″N, 107°39′1.1″E; Fig. 1). Over the last 50 years, Luochuan and Xifeng have experienced similar climatic conditions, with mean annual temperatures (MAT) of 9.6 °C and 8.7 °C; and mean annual precipitation (MAP) values of 607 mm and 547 mm, respectively. The meteorological data we used were taken from http://www.data.cma.cn. The modern vegetation of the central CLP can be characterized as typical temperate steppe and forest steppe. In the northwestern CLP, vegetation gradually transitions to temperate desert vegetation along with reduced precipitation (Cheng and Wan, 2002). Our loess samples were originally sampled at 2-cm intervals. Then, equal amounts of three consecutive samples taken every 25 cm were mixed, forming a sample with a total mass of 30 g. The mixed loess core samples were prepared for *n*-alkane extraction, gas chromatography and isotope analysis.

Each loess sample (~30 g) was extracted with a mixture of dichloromethane (DCM) and methanol (MeOH) (9:1, v/v) using Accelerated Solvent Extraction (ASE 350, Dionex™). Total extracted lipid compounds were transported *via* a soft N_2 stream. The alkane fractions in the sediment were separated by silica gel chromatography using hexane eluents (Liu and Huang, 2005; Wang et al., 2013). Gas chromatography (GC) was performed using an Agilent 6890 Series instrument equipped with a split-injector, HP-1ms GC column (60 m length; 0.32 mm i.d.; 0.25 μm film) and a flame ionization detector. For quantification, peak areas for *n*-alkanes were compared with those from an external standard mixture (C_{21}–C_{33}; odd carbon numbers). The samples were injected in split mode at an inlet temperature of 310 °C and a column flow rate of 1.2 ml/min. The analysis was run under the following temperature ramps: held for 1 min at an initial temperature of 40 °C; heated to 150 °C at 10 °C/min; and then heated to 310 °C at 6 °C/min and held for 20 min.

2.2. Analysis method

The compound-specific hydrogen isotope ratios were measured using a Delta-V IRMS (Thermo-Finnigan). Approximately 300 ng of *n*-alkane was injected into a Thermo Trace GC in splitless mode. The temperature ramps were the same as those used in the GC analysis. The *n*-alkanes were converted to hydrogen gas using a high-temperature pyrolysis reactor at 1430 °C. During all the experiments, the H_3^+ factor was 1.83 ± 0.03 for each week. The stability of the isotope mass spectrometer (with nine groups of reference gas tests) was better than 0.04‰. Mixed laboratory standards of *n*-alkanes (odd carbon number *n*-alkanes; C_{21}–C_{33}; Sigma-Aldrich) were measured after every four injections to monitor the external precision of the hydrogen isotope analysis, and the standard deviation of the working standard was < 2‰. The working standard was calibrated using Indiana University FAME reference substances. The GC analyses and compound-specific hydrogen isotope analyses were performed at the Stable Isotope Laboratory of the Institute of the Earth Environment, Chinese Academy of Sciences (IEE-CAS).

3. Results and discussion

3.1. Magnetic susceptibility chronologies

The chronologies of the two loess-paleosol sequences were established using 2-cm interval magnetic susceptibility data based on the orbital tuning method (Kukla et al., 1988; Ding et al., 1994). The magnetic susceptibility records for the period since 130 ka BP for Xifeng were taken from Liu and Huang (2005). The loess core magnetic susceptibility curves for this study were then compared with the records from previous studies for Xifeng (Guo et al., 2009; Hao et al., 2012) and Luochuan (An et al., 1990; Hao et al., 2012). All the data for the central CLP were consistent when using the magnetic susceptibility-based age model (Fig. 2).

3.2. δD_{wax} records from Xifeng and Luochuan

The δD_{wax} records from Xifeng and Luochuan fluctuate consistently over the last 250 ka. These trends are somewhat similar to the sites' loess magnetic susceptibility curves (Fig. 3). Depleted δD_{wax} values correspond to relatively high magnetic susceptibility, and enriched δD_{wax} values correspond to relatively low magnetic susceptibility. The mean sampling interval in our loess δD_{wax} records was 2.6 ka. Based on the Fourier transform (Mudelsee, 2013) and wavelet methods (Torrence and Compo, 1998), the original δD_{wax} series were interpolated to 3-ka

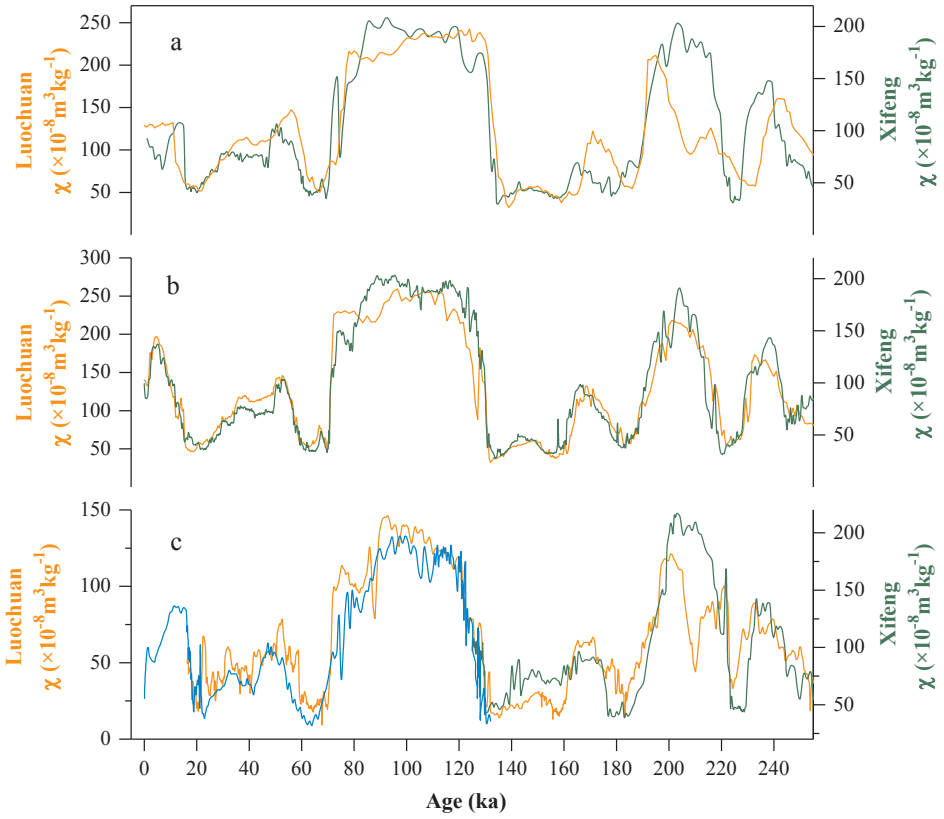

Fig. 2. Magnetic susceptibility of the Xifeng and Luochuan cores. a, orange line, Luochuan profile (An et al., 1990), green line, Xifeng (Guo et al., 2009); b, Xifeng and Luochuan profiles (Hao et al., 2012); c, blue line, Xifeng Profile since 130 ka BP (Liu and Huang, 2005), green and orange line, XFJ3 and LC3J cores from Xifeng and Luochuan, respectively (this study). (For interpretation of the references to color in this figure legend, the reader is referred to the web version of this article.)

interval series to perform period analysis. Both records exhibited significant ~100-ka, ~40-ka and ~20-ka cycles (Fig. 4a and b). These periodic characteristics are ubiquitous in other loess records, *e.g.*, $\delta^{13}C_{ic}$ (carbon isotopes of inorganic carbonate), grain size and magnetic susceptibility (Sun et al., 2012, 2015; Hao et al., 2012). Overall, the δD_{wax} records for the central CLP can be described as an ordered oscillation with three periods and an amplitude at the glacial-interglacial scale of ± 15‰.

Based on the large-scale water balance between land and sea, a stronger summer monsoon can transport more moisture from the western Pacific and Indian oceans to the ASM region. This process results in a more humid climate and depleted isotopic values in precipitation (Liu et al., 2014b). However, because of the complicated isotopic fractionation processes between the isotopic composition of precipitation (δD_{prec}) and δD_{wax} (Gat, 1996; Sessions et al., 1999), δD_{wax} records can be interpreted only as a composite signal of climatological and ecological change. In principle, rain falls to the ground and enters the soil as soil moisture, and plants take up this soil water. Thus, the δD_{wax} values of leaf *n*-alkanes or *n*-acids inherit the isotopic composition characteristics of the soil water (Sachse et al., 2012). Consequently, δD_{wax} values are considered to be controlled by the combined impact of δD_{prec} values, fractionation between precipitation and soil water ($\varepsilon_{sw\text{-}p}$), which is controlled by evaporation (McInerney et al., 2011), and fractionation between δD_{wax} values and the isotopic value of the source water ($\varepsilon_{wax\text{-}sw}$), which is in turn controlled by the type of plant growth (Liu and Yang, 2008). δD_{prec} values are considered the primary controlling factor (Sachse et al., 2012). The isotopic composition of the moisture source, local condensation temperature and precipitation conspire to affect δD_{prec} values (Gat, 1996). $\varepsilon_{wax\text{-}sw}$ values vary among vegetation and ecological types, and this variation greatly affects δD_{wax} values (Liu and Yang, 2008). The δD_{wax} values of forests differ greatly from those of grasslands, for example, even if they share the same local δD_{prec} values. Thus, the combined effect of climatological and ecological factors determines the δD_{wax} record. These influential factors can be further summarized into four groups: isotopic composition of the source; temperature; precipitation; and vegetation type. To extract a single factor from δD_{wax} records, *e.g.*, the amount of precipitation, the other effects should be eliminated *via* calibration (Tierney and deMenocal, 2013; Thomas et al., 2014).

3.3. Elimination of the effect of ice volume and temperature on δD_{wax}

Different ice volumes during glacial and interglacial stages can cause changes in the isotopic composition of seawater. Thus, the ice volume effect should first be removed from loess δD_{wax} data. Changes in global ice volumes have been estimated using marine benthic $\delta^{18}O$ records (Lisiecki and Raymo, 2005). Precipitation isotope data from GNIP stations (http://www-naweb.iaea.org) indicate that the relation between the $\delta^{18}O$ and δD values of precipitation on the CLP can be expressed as $\delta D_{prec} = 6.9 \times \delta^{18}O_{prec}$ (Fig. 5a). The local meteoric water line (LMWL) of the CLP is close to that of northwestern China ($\delta D = 7.4 \times \delta^{18}O + 1.4$, Liu et al., 2014a) and the global meteoric water line (GMWL) (Gat, 1996). In this study, therefore, we used 7.4 to convert $\delta^{18}O_{prec}$ to δD, and followed the ice volume calibration method of Tierney and deMenocal (2013). The ice volume calibration did not change the overall trend of the original loess δD_{wax} record (Fig. 5b), implying that sea water isotope variations were not the predominant factor affecting δD_{wax} values in the central CLP.

Local temperature affects isotopic fractionation during precipitation condensation (Gat, 1996). Global precipitation isotope patterns also show a significant temperature effect (Bowen, 2010). In previous studies, the temperature effect was removed from the original δD_{wax} signal so that the hydrogen isotopic records could be used as hydroclimatic proxies (Thomas et al., 2014). On the CLP, the loess GDGT index can be used as a potential air temperature proxy (Gao et al., 2012; Peterse et al., 2014; Yang et al., 2014; Lu et al., 2016; Tang et al., 2017). Based on a comparison of GDGTs-derived temperatures with sea surface temperatures (SSTs) from the South China Sea (Herbert et al., 2010), CLP temperatures appear similar to low-latitude SSTs (Fig. 6a). Additionally, MAT values for Xifeng on the CLP and for Guangzhou in

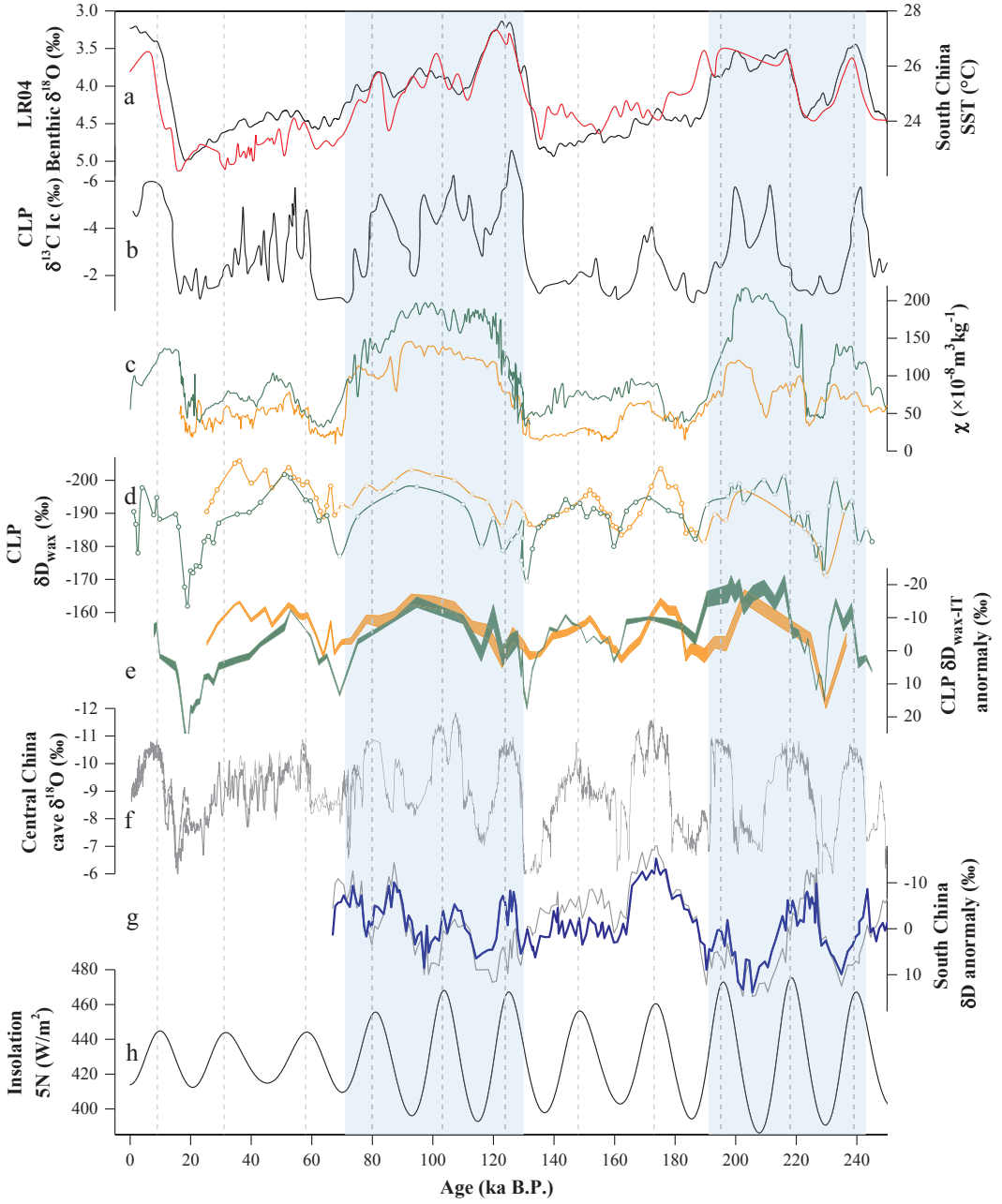

Fig. 3. Comparison of various isotopic records with SSTs, ice volume, and insolation. a, Marine benthic $\delta^{18}O$ (black line; Lisiecki and Raymo, 2005) and SST records from the South China Sea (red line; Herbert et al., 2010); b, loess $\delta^{13}C_{ic}$ values as a record of summer precipitation (Sun et al., 2015); c, magnetic susceptibility records from Xifeng (green line) and Luochuan (orange line, this study); d, δD_{wax} records from Xifeng and Luochuan (this study); e, $\delta D_{wax\text{-}IT}$ records as a proxy for hydroclimatic humid/arid conditions in the central CLP; f, stalagmite $\delta^{18}O$ records from central China (gray line; Sanbao and Linzhu caves; Wang et al., 2008; Cheng et al., 2009); g, δD_{wax} (gray line) and $\delta D_{wax\text{-}IT}$ (blue line) records employed as hydroclimatic proxies for southern China (Thomas et al., 2014); h, July 5°N insolation (Laskar et al., 2004), where the dotted lines mark the ages of the insolation maxima.(For interpretation of the references to color in this figure legend, the reader is referred to the web version of this article.)

southern China show the same trend over a decadal scale (Fig. 6b). Using this information, we can estimate relative changes in temperature before 110 ka BP on the CLP based on South China Sea SSTs. The relation 0.27–0.37‰ $\delta^{18}O_{prec}$/°C has been used in northern and western China (Liu et al., 2014a) to remove the temperature effect. The relation between $\delta^{18}O_{prec}$ and temperature was converted to δD_{prec} *versus* temperature using a factor of 7.4 (Liu et al., 2014a). The removal of the temperature effect followed the approach used by Thomas et al. (2014), with a calibrated uncertainty of ± 1σ standard deviation (Fig. 3). For our current calibration, only the temperature effect of condensation was removed. Any potential isotopic fractionation during evaporation in the moisture source region and in the local soil could not be considered; the response of the δD_{wax} records to these two processes was therefore also difficult to estimate accurately. However, because higher temperatures would cause higher isotopic values in both of these processes and a wider calibration range would need to be chosen to remove the influence of temperature, we think it possible that evaporation may retain some effect. After removing the ice volume and temperature effects ($\delta D_{wax\text{-}IT}$), our $\delta D_{wax\text{-}IT}$ curve was not significantly different from the original δD_{wax} curve. Assuming that the moisture transported to the central CLP has come from a relatively stable source, the $\delta D_{wax\text{-}IT}$ record would appear to be principally related to variations in precipitation and vegetation in the central CLP.

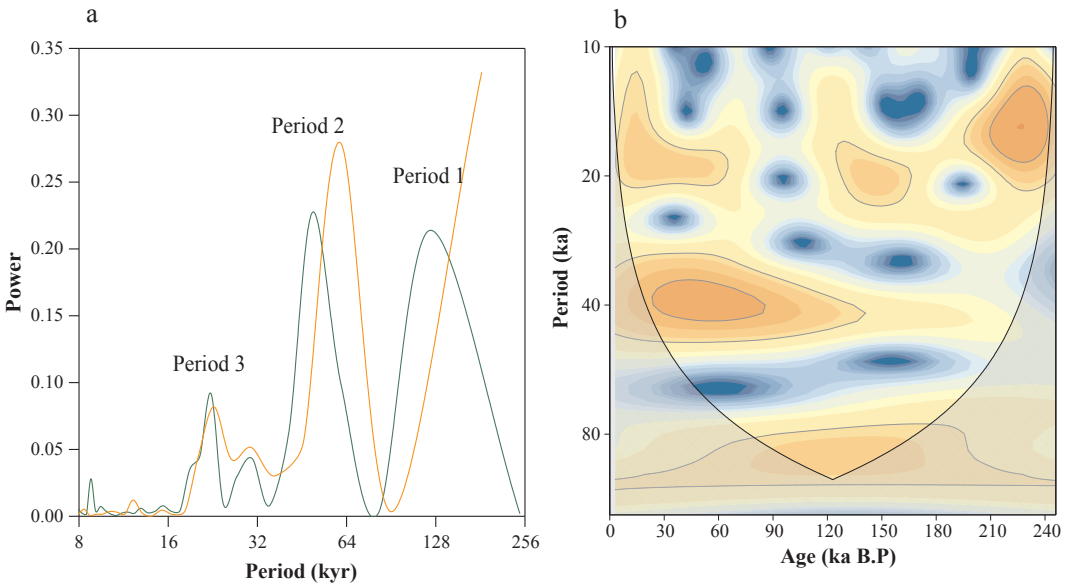

Fig. 4. Fourier period and wavelet spectrum analysis results derived from the δD_{wax} records for Xifeng and Luochuan, central CLP. a, Fourier spectrum period for Xifeng (green line) and Luochuan (orange line) showed ~100-ka, ~40-ka and ~20-ka cycles; b, wavelet power spectrum results three cycles of δD_{wax} records. The thick gray contour designated the 5% significance level against red noise and the cone of influence (COI). (For interpretation of the references to color in this figure legend, the reader is referred to the web version of this article.)

3.4. Influence of precipitation amount and vegetation type on the CLP's δD_{wax} records

$\delta^{18}O_{prec}$ data for the CLP show a significant negative correlation with summer precipitation values (nine stations; monthly data from Jun-Aug from GNIP and CHNIP stations; http://www-naweb.iaea.org and Liu et al., 2014a; Fig. 7). Because precipitation on the CLP mainly comes from summer rainfall (Yan, 2015), the CLP δD_{wax} records likely contain a precipitation amount effect, *i.e.*, large amounts of precipitation result in lower δD_{wax} values. Additionally, changes in precipitation also lead to changes in vegetation. Current MAP values for the central CLP range from 300 mm to 600 mm, and the vegetation zone can be characterized as temperate steppe. With a decrease in precipitation, plants in the more arid northwestern CLP gradually transition to desert vegetation (Cheng and Wan, 2002). Reconstructed results suggest that fluctuations in MAP values for the CLP would likely have ranged from 200 mm to 700 mm over an glacial-interglacial scale (Zhou et al., 2010, 2015; Sun et al., 2015), meaning that vegetation type would have changed from desert shrub, to steppe, or even to forest-steppe. Numerous studies have confirmed the effect of plant type on δD_{wax} values (Liu and Yang, 2008; Sachse et al., 2012). Both precipitation amount and vegetation type would therefore have influenced the CLP's δD_{wax} records.

Despite the combined effect of precipitation and vegetation type, these two individual factors have a similar isotopic effect on the central CLP: increasing precipitation and the corresponding vegetation transition to grassland cause lower δD_{wax} values; decreasing precipitation and the corresponding desert-shrub expansion cause higher δD_{wax} values. We would therefore suggest that the $\delta D_{wax\text{-}IT}$ record can be used as an environmental moisture proxy in the central CLP to obtain combined climatic and ecological information (Liu and Huang, 2005).

3.5. Hydroclimatic variability in the central CLP over a 20-ka cycle

Comparing $\delta D_{wax\text{-}IT}$, magnetic susceptibility and loess $\delta^{13}C_{ic}$ values (Sun et al., 2015), it becomes clear that these records are consistent in terms of environmental humidity, summer monsoonal strength and summer precipitation, demonstrating that the hydrological changes observed in the central CLP were predominantly controlled by the ASM. Because the $\delta D_{wax\text{-}IT}$ record for the CLP, the stalagmite $\delta^{18}O$ record for

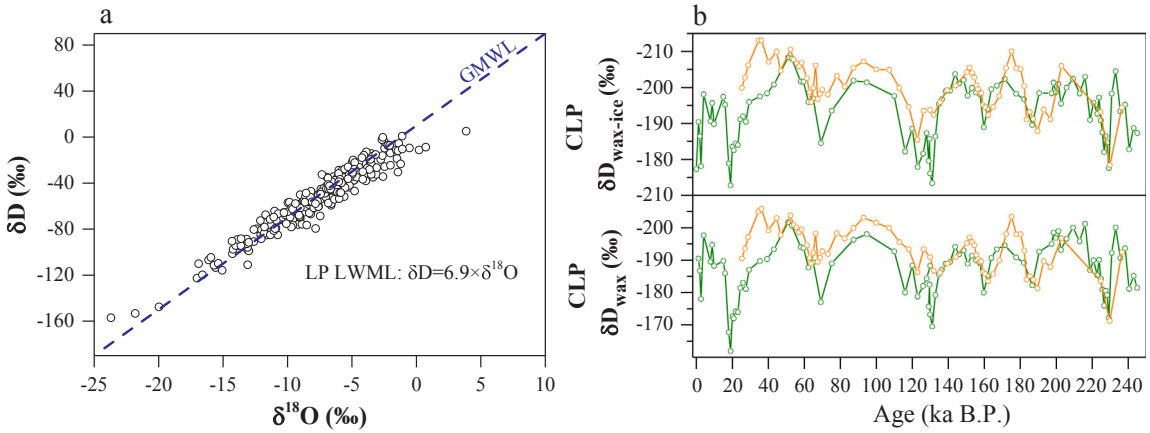

Fig. 5. Global meteoric water line (GMWL) and local meteoric water line (LMWL) for the CLP; b, δD_{wax} and $\delta D_{wax\text{-}ice}$ records from Xifeng (green line) and Luochuan (orange line). (For interpretation of the references to color in this figure legend, the reader is referred to the web version of this article.)

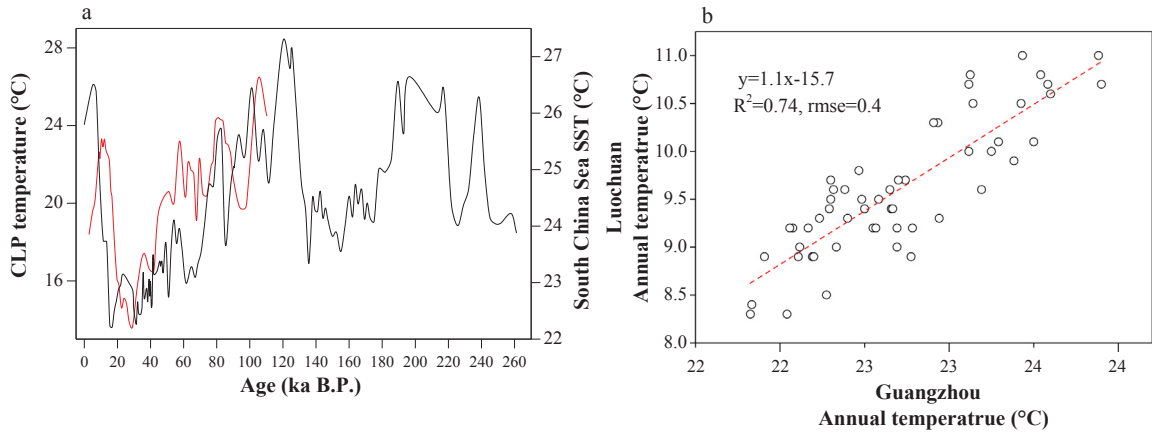

Fig. 6. Comparison of CLP temperatures and South China Sea SSTs. a, SST record from the South China Sea (black line; Herbert et al., 2010) and GDGT-reconstructed air temperatures for the CLP (red line; Gao et al., 2012); b, relation between MAT values for the last 50 yr for the central CLP (Luochuan) and South China (Guangzhou). (For interpretation of the references to color in this figure legend, the reader is referred to the web version of this article.)

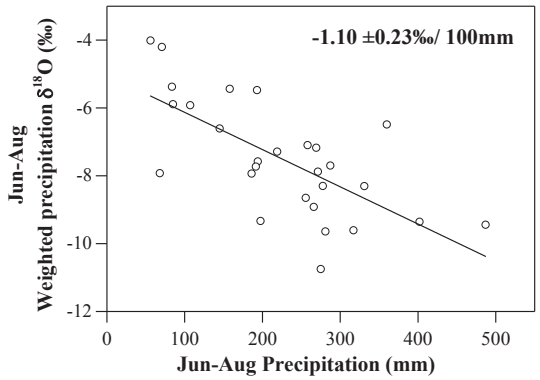

Fig. 7. The negative correlation between weighted $\delta^{18}O_{prec}$ values and summer precipitation values (Jun-Aug) for the CLP. The data are taken from nine GNIP and CHNIP stations (http://www-naweb.iaea.org; Liu et al., 2014a).

central China (Wang et al., 2008; Cheng et al., 2009), and the δD_{wax} record for southern China (Thomas et al., 2014) are all related to local precipitation values, we compared these records to identify regional hydroclimatic differences. The stalagmite $\delta^{18}O$ records from southern and central China, and the δD_{wax} record from southern China, all contain precessional signals (Wang et al., 2008; Cheng et al., 2009, 2016; Thomas et al., 2014). Despite our low sample resolution for the central CLP (with a mean interval of ~2.6 ka), ~20-ka precessional cycles were also present in the $\delta D_{wax\text{-}IT}$ record (Fig. 3). Cross wavelet analysis (Grinsted et al., 2004) of the CLP $\delta D_{wax\text{-}IT}$ records yielded significant correlations with insolation (Jul 5°N, Laskar et al., 2004) and the stalagmite $\delta^{18}O$ record (Wang et al., 2008; Cheng et al., 2009) over ~20 ka cycles (Fig. 8a and b). Thus, solar insolation during the precessional cycle directly forced summer monsoonal precipitation variability in southern China, central China, and even the central CLP.

Because the original time series contained multi-cycle signals, we used the FFT filter method to separate hydroclimatic variability during precessional cycles. The ~20-ka signal in the central CLP, central China and southern China showed good synchronization with summer insolation, and the isotopic minima approximately matched the insolation maxima (Fig. 9a). Therefore, solar insolation is related to summer monsoonal precipitation; increasing insolation would have caused more rainfall, resulting in a more humid environment. However, the different amplitudes and phases of the ~20-ka cyclical signals in the three locations reflect different responses of ASM precipitation to changes in insolation. For instance, the stalagmite $\delta^{18}O$ record is almost fully synchronized with insolation fluctuations, with a phase lag between them of < 10°. In contrast, the $\delta D_{wax\text{-}IT}$ records in the CLP and southern China feature a slight phase lag or advance. The CLP $\delta D_{wax\text{-}IT}$ minima were ~55° (~3 ka) behind the insolation maxima (Fig. 9b), and the

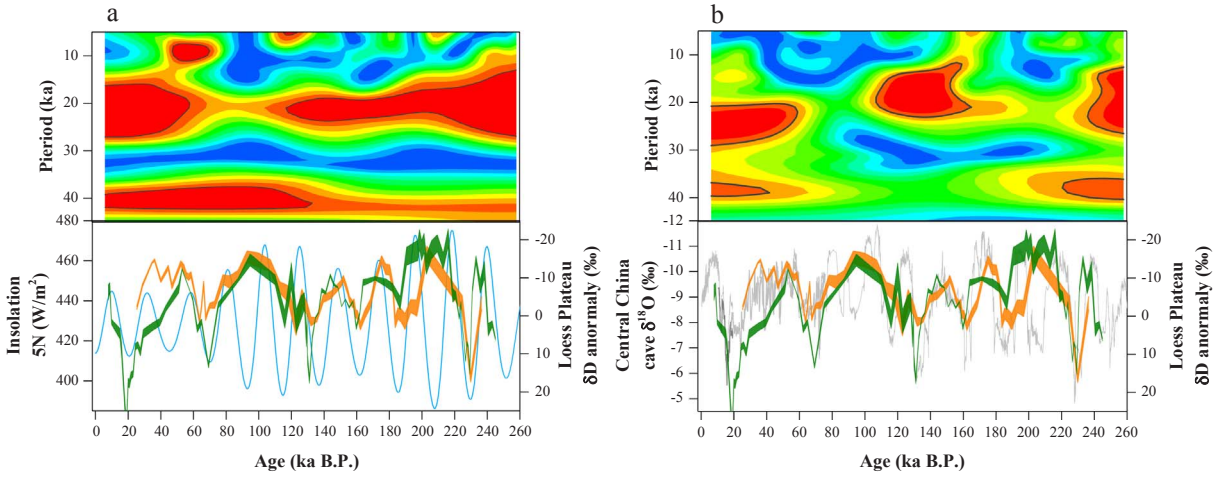

Fig. 8. Cross Wavelet Transform between CLP $\delta D_{wax\text{-}IT}$ values and central China stalagmite $\delta^{18}O$ values, and summer insolation. a, blue line, July 5°N insolation (Laskar et al., 2004), green and orange line, CLP $\delta D_{wax\text{-}IT}$ (this study); b, gray line, central China stalagmite $\delta^{18}O$ records (Wang et al., 2008; Cheng et al., 2009), green and orange line, CLP $\delta D_{wax\text{-}IT}$ (this study). (For interpretation of the references to color in this figure legend, the reader is referred to the web version of this article.)

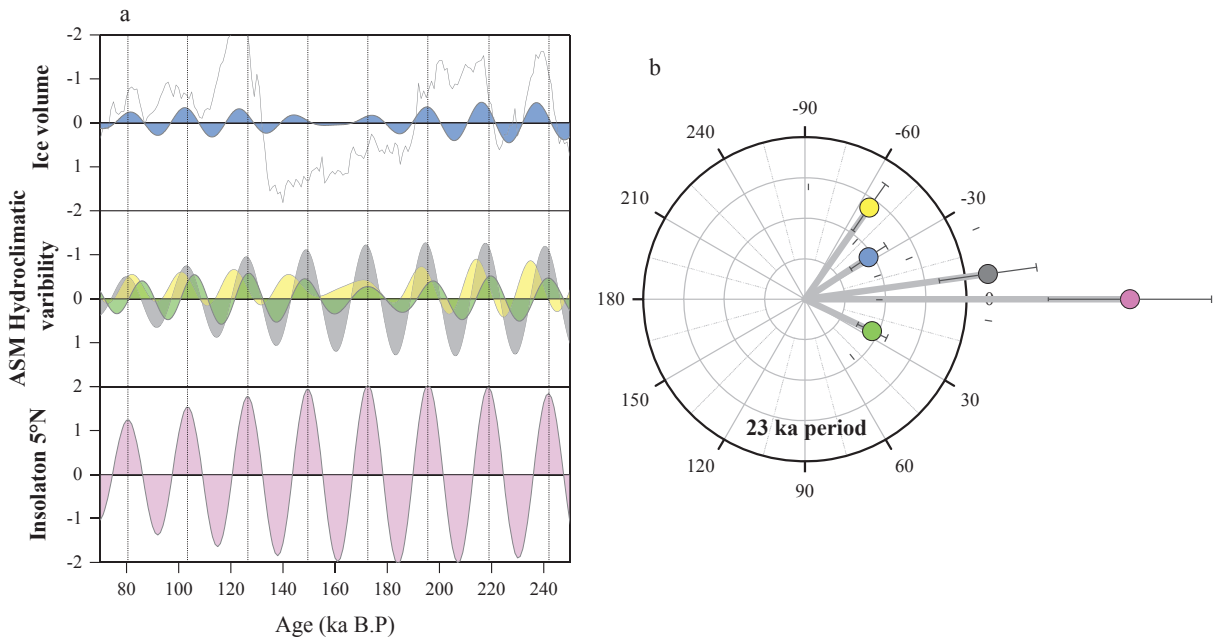

Fig. 9. Isotopic hydroclimatic variability in the CLP, central China and southern China. a, FFT filter signal of various records over a 21–23-ka frequency, shown in units of standard deviation (σ); b, hydroclimatic variability over a 23-ka cycle. The radius represents the amplitude of each signal, with 1 unit radius equivalent to 0.25 σ amplitude. Pink color: July 5°N insolation; gray color: stalagmite $\delta^{18}O$ records from central China; green color: hydroclimatic $\delta D_{wax\text{-}IT}$ records from southern China; yellow color: hydroclimatic $\delta D_{wax\text{-}IT}$ records from the central CLP; blue color: ice volume. (For interpretation of the references to color in this figure legend, the reader is referred to the web version of this article.)

southern China $\delta D_{wax\text{-}IT}$ record was slightly advanced relative to solar insolation. Thomas et al. (2014) suggested that the phase difference in the ~20-ka cycle between central China and southern China resulted from the strong influence of ice volumes or glacial boundary conditions on the stalagmite $\delta^{18}O$ record. This hypothesis may also explain the larger phase lag in the CLP $\delta D_{wax\text{-}IT}$ record, because the CLP was more strongly affected by the ice sheet than were regions at lower latitudes.

Nevertheless, the influence of ice volumes or glacial boundary conditions does not entirely explain the amplitudinal differences between these regions. As glacial retreat and enhanced insolation would have caused more intense hydroclimatic fluctuations in this ASM-marginal region, the amplitudes present in the CLP sections should not be smaller than those found in other regions. However, the larger amplitudes in the stalagmite $\delta^{18}O$ record of central China appear to be in conflict with the previous hypothesis. We therefore inferred that the different hydroclimatic responses of the stalagmite $\delta^{18}O$ and $\delta D_{wax\text{-}IT}$ records can be explained in part by these amplitudinal differences. In the central CLP and southern China, the isotopic records derived from plant $\delta D_{wax\text{-}IT}$ values can be used to compare the amplitudes of fluctuations in hydroclimatic variability over a 20-ka cycle. The hydroclimatic changes over the course of a 20-ka cycle appear to have been primarily controlled by the strength of the ASM; the combined effect of insolation forcing and ice volume changes influenced humidity in the central CLP.

3.6. Glacial-interglacial hydroclimatic differences between the central CLP and southern China

The hydroclimatic changes recorded in the ASM region differ markedly between glacial and interglacial periods. Generally low $\delta D_{wax\text{-}IT}$ values in the central CLP indicate that this ASM-marginal region was dominated by a wet climate during interglacial periods (Fig. 3), in agreement with the high magnetic susceptibility and negative $\delta^{13}C_{ic}$ values of the region's interglacial loess records. However, the overall trend in $\delta D_{wax\text{-}IT}$ values during interglacial periods in southern China is relatively positive (Thomas et al., 2014). Although the $\delta D_{wax\text{-}IT}$ records are not long enough to discuss cyclic characteristics over a 100-ka period, an overall inverse isotopic trend during the warm periods of MIS 5 and MIS 7 can be observed (Fig. 3). Therefore, hydroclimatic variability in the central CLP and southern China can be taken as having been similar over a ~20-ka cycle, but inverse on a glacial-interglacial timescale. We believe this discrepancy to be key to revealing the various regional hydrological changes evident across the ASM region.

Chinese decadal meteorological records have revealed different precipitation patterns over recent years. Precipitation levels at Xifeng and Luochuan have continually declined since the 1980s, whereas precipitation at Guangzhou has increased (Fig. 10). Decadal variability in monsoonal strength may be the main factor driving recent inverse precipitation phases in northern and southern China (Ding et al., 2008). We suspect that, due to obvious cyclical temperature fluctuations during the 100-ka cycle since the late Pleistocene (Jouzel et al., 2007; Herbert et al., 2010), a warmer climate during interglacials has caused a stronger summer monsoon and pushed the rainbelt northward (Broecker and Putnam, 2013; Yang et al., 2015). A more northerly rainbelt has therefore resulted in greater precipitation and lower isotopic values in the CLP. In contrast, relatively less rainfall with higher isotopic values has fallen in southern China. We can therefore safely assume that the relative differences in the changes to precipitation seen in northern and southern China, as caused by monsoonal variability, may partly explain the differences in the north-south $\delta D_{wax\text{-}IT}$ values observed over a glacial-interglacial scale. However, transgressions and regressions may have also greatly affected hydroclimatic conditions during glacial and interglacial periods. During interglacials, a coastline lying farther to the north would have led to higher precipitation isotopic values in the coastal regions of southern China. This change in the geographical location of the land in relation to the sea may also have led to changes in regional monsoonal circulation patterns; the moisture sources (*i.e.*, the western Pacific and Indian oceans) would have then contributed further to the regional hydroclimatic differences recorded (Cai et al., 2015). On the CLP, which is relatively far inland, the isotopic values of precipitation would have been less affected by such locational shifts in the land in relation to the sea, and therefore by any possible changes in moisture sources; this would mean that CLP $\delta D_{wax\text{-}IT}$ values would have been more closely related to changes in the ASM.

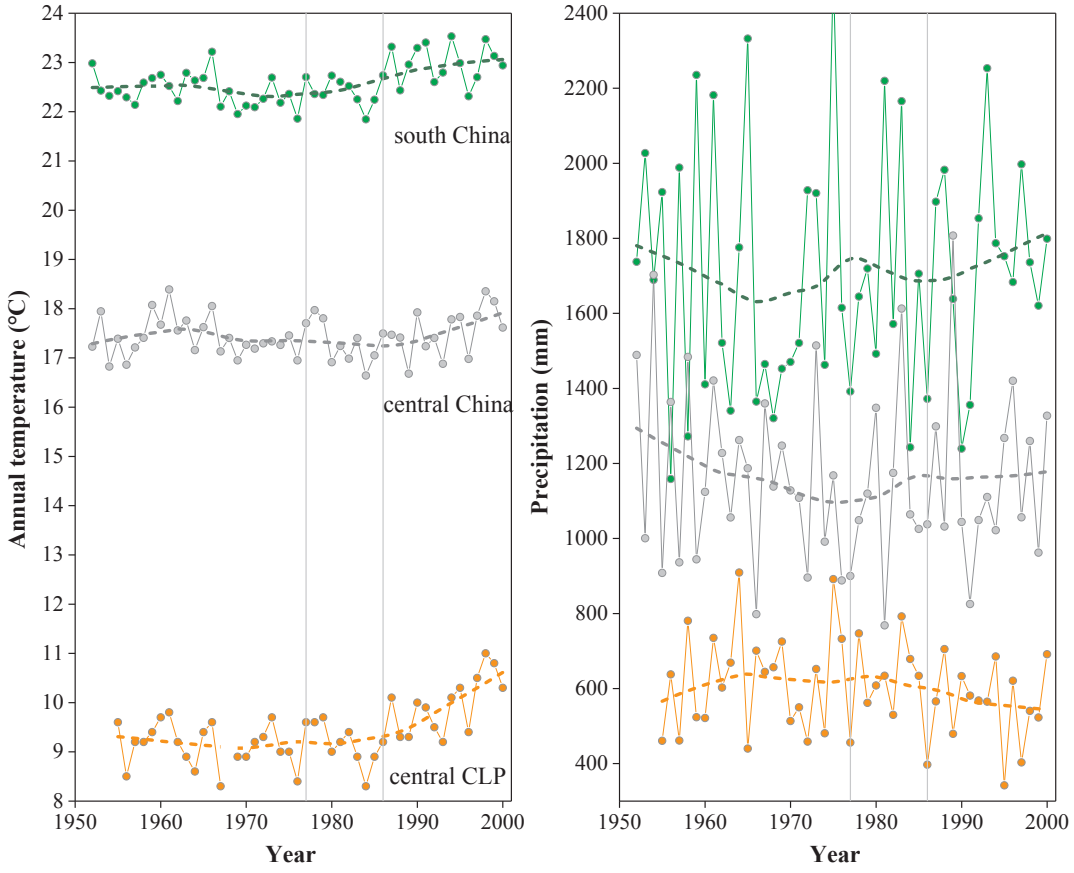

Fig. 10. MAT and MAP records for Luochuan (central CLP), Yichang (central China) and Guangzhou (southern China) for the years 1950–2000. The dotted lines show 20-yr smoothing trends.

3.7. Hydroclimatic changes on the CLP in relation to global warming

Any interpretation of the different precipitation patterns found in China is bound to be complex. However, our loess δD_{wax} records would indicate that the changes between dry and wet environments seen in the central CLP were, and are, strictly controlled by summer monsoonal precipitation. An enhanced monsoon, whether over a ~20-ka cycle or across a glacial-interglacial scale, delivers more rainfall to the margins of the monsoon zone, resulting in a more humid environment. Current MAP in the central CLP is only 500 mm, corresponding to the low-insolation, low-humidity stage of an interglacial period. The constant trend toward drought in this region over recent years has been, and is, detrimental to the ecological environment as well as to humankind. In these circumstances, an enhanced summer monsoon becomes essential for alleviating drought in this region. Due to the excessive emission of greenhouse gases, the Earth is entering an artificially warm period. In a certain sense, changing the heat balance through human activity will be conducive to strengthening the monsoon and mitigating drought on the CLP (Yang et al., 2015). The climate report issued by the Pachauri et al. (2014) also predicts that CLP precipitation may increase as the climate warms. We would therefore recommend that global responses to climate change should take full account of the regional imbalance in water distribution and equilibrium between arid ASM-marginal regions and typically humid ASM regions.

4. Conclusions

In this study, two loess δD_{wax} series from the central CLP were used to reconstruct the paleo-hydroclimatic variability of a marginal region of the ASM over the last 250 ka. Arid/humid alternations followed changes in the summer monsoon and monsoonal rainfall on the CLP, indicating that monsoonal intensity exerts the primary control on regional hydroclimatic changes. Over a ~20-ka period, consistent hydroclimatic changes in the central CLP, central China and southern China were related to similar solar insolation effects on the summer monsoon in the three regions. However, dramatic changes in the position of the land and sea may have affected the hydroclimatic variability in coastal areas more than in areas farther inland. An alleviation of the drying trend in ASM-marginal regions caused by the strengthening of the monsoon and a northward shift in the rainfall belt due to climate warming should be taken into account when developing strategies to respond to global warming. This alleviation of drought would be beneficial to the fragile ecological environment of the CLP as well as to the 200 million people who live there.

Acknowledgements

Authors would like to thank Prof. Jimin Sun and an anonymous reviewer for their constructive comments. This work was supported by the National Key Funds of China (Grant No. 2013CB955900) and National Natural Science Foundation of China (Grant Nos. 41473022, 41773010).

References

An, Z.S., 2000. The history and variability of the East Asian paleomonsoon climate. Quat. Sci. Rev. 19, 171–187.
An, Z.S., Liu, T.S., Lu, Y.C., Porter, S.C., Kukla, G., Wu, X.H., Hua, Y.M., 1990. The long-term paleomonsoon variation recorded by the loess-paleosol sequence in central China. Quat. Int. 7, 91–95.
Bowen, G.J., 2010. Isoscapes: spatial pattern in isotopic biogeochemistry. Annu. Rev. Earth Planet. Sci. 38, 161–187.
Broecker, W.S., Putnam, A.E., 2013. Hydrologic impacts of past shifts of Earth's thermal equator offer insight into those to be produced by fossil fuel CO_2. Proc. Natl. Acad.

Sci. U.S.A. 110, 16710–16715.
Cai, Y.J., Fung, I.Y., Edwards, R.L., An, Z.S., Cheng, H., Lee, J.E., Tan, L.C., Shen, C.C., Wang, X.F., Day, J.A., 2015. Variability of stalagmite-inferred Indian monsoon precipitation over the past 252,000 y. Proc. Natl. Acad. Sci. U.S.A. 112, 2954–2959.
Cheng, H., Edwards, R.L., Broecker, W.S., Denton, G.H., Kong, X.G., Wang, Y.G., Zhang, R., Wang, X.F., 2009. Ice age terminations. Science 326, 248–252.
Cheng, H., Edwards, R.L., Sinha, A., Spötl, C., Yi, L., Chen, S.T., Kelly, M., Kathayat, G., Wang, X.F., Li, X.L., Kong, X.G., Wang, Y.J., Ning, Y.F., Zhang, H.W., 2016. The Asian monsoon over the past 640,000 years and ice age terminations. Nature 534, 640. http://dx.doi.org/10.1038/nature18591.
Cheng, J.M., Wan, H., 2002. Vegetation Construction and Soil and Water Conservation in the Loess Plateau of China. China Forestry Publishing House, Beijing.
Ding, Y.H., Wang, Z.Y., Sun, Y., 2008. Inter-decadal variation of the summer precipitation in East China and its association with decreasing Asian summer monsoon. Part I: observed evidences. Int. J. Climatol. 28, 1139–1161.
Ding, Z.L., Yu, Z.W., Rutter, N.W., Liu, T.S., 1994. Towards an orbital time scale for Chinese loess deposits. Quat. Sci. Rev. 13, 39–70.
Gao, L., Nie, J.S., Clemens, S.C., Liu, W.G., Sun, J.M., Zech, R., Huang, Y.S., 2012. The importance of solar insolation on the temperature variations for the past 110 kyr on the Chinese Loess Plateau. Palaeogeogr. Palaeoclimatol. Palaeoecol. 317–318, 128–133.
Gat, J.R., 1996. Oxygen and hydrogen isotopes in the hydrologic cycle. Annu. Rev. Earth Planet. Sci. 24, 225–262.
Grinsted, A., Moore, J.C., Jevrejeva, S., 2004. Application of the cross wavelet transform and wavelet coherence to geophysical time series. Nonlinear Proc. Geoph. 11, 561–566.
Guo, Z.T., Berger, A., Yin, Q.Z., Qin, L., 2009. Strong asymmetry of hemispheric climates during MIS-13 inferred from correlating China loess and Antarctica ice records. Clim. Past 5, 21–31.
Hao, Q.Z., Wang, L., Oldfield, F., Peng, S.Z., Qin, L., Song, Y., Xu, B., Qiao, Y.S., Bloemendal, J., Guo, Z.T., 2012. Delayed build-up of Arctic ice sheets during 400,000-year minima in insolation variability. Nature 490, 393–396.
Herbert, T.D., Peterson, L.C., Lawrence, K.T., Liu, Z.H., 2010. Tropical ocean temperatures over the past 3.5 million years. Science 328, 1530–1534.
Hou, J.Z., D'Andrea, W.J., MacDonald, D., Huang, Y.S., 2007. Hydrogen isotopic variability in leaf waxes among terrestrial and aquatic plants around Blood Pond, Massachusetts (USA). Org. Geochem. 38, 977–984.
Jouzel, J., Masson-Delmotte, V., Cattani, O., Dreyfus, G., Falourd, S., Hoffmann, G., Minster, B., Nouet, J., Barnola, J.M., Chappellaz, J., Fischer, H., Gallet, J.C., Johnsen, S., Leuenberger, M., Loulergue, L., Luethi, D., Oerter, H., Parrenin, F., Raisbeck, G., Raynaud, D., Schilt, A., Schwander, J., Selmo, E., Souchez, R., Spahni, R., Stauffer, B., Steffensen, J.P., Stenni, B., Stocker, T.F., Tison, J.L., Werner, M., Wolff, E.W., 2007. Orbital and millennial antarctic climate variability over the Past 800,000 years. Science 317, 793–796.
Kukla, G., Heller, F., Liu, X.M., Xu, T.C., Liu, T.S., An, Z.S., 1988. Pleistocene climates in China dated by magnetic susceptibility. Geology 16, 811–814.
Laskar, J., Robutel, P., Joutel, F., Gastineau, M., Correia, A., Levrard, B., 2004. A long-term numerical solution for the insolation quantities of the Earth. Astron. Astrophys. 428, 261–285.
Lisiecki, L.E., Raymo, M.E., 2005. A Pliocene-Pleistocene stack of 57 globally distributed benthic $\delta^{18}O$ records. Paleoceanography 20, PA1003. http://dx.doi.org/10.1029/2004PA001071.
Liu, J.R., Song, X.F., Yuan, G.F., Sun, X.M., 2014a. Stable isotopic compositions of precipitation in China. Tellus B 66, 22567. http://dx.doi.org/10.3402/tellusb.v66.22567.
Liu, T.S., Ding, Z.L., Guo, Z.T., 1991. Loess, Environment, and Global Change. Science Press, Beijing.
Liu, W.G., Huang, Y.S., 2005. Compound specific D/H ratios and molecular distributions of higher plant leaf waxes as novel paleoenvironmental indicators in the Chinese Loess Plateau. Org. Geochem. 36, 851–860.
Liu, W.G., Yang, H., 2008. Multiple controls for the variability of hydrogen isotopic compositions in higher plant n-alkanes from modern ecosystems. Global Change Biol. 14, 2166–2177.
Liu, Z.Y., Wen, X.Y., Brady, E.C., Otto-Bliesner, B., Yu, G., Lu, H.Y., Cheng, H., Wang, Y.J., Zheng, W.P., Ding, Y.H., Edwards, R.L., Cheng, J., Liu, W., Yang, H., 2014b. Chinese cave records and the East Asia Summer Monsoon. Quat. Sci. Rev. 83, 115–128.
Lu, H.X., Liu, W.G., Wang, H.Y., Wang, Z., 2016. Variation in 6-methyl branched glycerol dialkyl glycerol tetraethers in Lantian loess–paleosol sequence and effect on paleotemperature reconstruction. Org. Geochem. 100, 10–17.
McInerney, F.A., Helliker, B.R., Freeman, K.H., 2011. Hydrogen isotope ratios of leaf wax n-alkanes in grasses are insensitive to transpiration. Geochim. Cosmochim. Acta 75, 541–554.
Mudelsee, M., 2013. Climate Time Series Analysis. Springer, Dordrecht. http://dx.doi.org/10.1007/978-90-481-9482-7.
Pachauri, R.K., Allen, M.R., Barros, V., Broome, J., Cramer, W., Christ, R., Church, J., Clarke, L., Dahe, Q., Dasgupta, P., 2014. Climate change 2014: synthesis report. Contribution of working groups I, II and III to the fifth assessment report of the intergovernmental panel on climate change. IPCC.
Peterse, F., Martínez-García, A., Zhou, B., Beets, C.J., Prins, M.A., Zheng, H.B., Eglinton, T.I., 2014. Molecular records of continental air temperature and monsoon precipitation variability in East Asia spanning the past 130,000 years. Quat. Sci. Rev. 83, 76–82.
Sachse, D., Billault, I., Bowen, G.J., Chikaraishi, Y., Dawson, T.E., Feakins, S.J., Freeman, K.H., Magill, C.R., McInerney, F.A., van der Meer, M.T.J., Polissar, P., Robins, R.J., Sachs, J.P., Schmidt, H.L., Sessions, A.L., White, J.W.C., West, J.B., Kahmen, A., 2012. Molecular paleohydrology: interpreting the hydrogen-isotopic composition of lipid biomarkers from photosynthesizing organisms. Annu. Rev. Earth Planet. Sci. 40, 221–249.
Sessions, A.L., Burgoyne, T.W., Schimmelmann, A., Hayes, J.M., 1999. Fractionation of hydrogen isotopes in lipid biosynthesis. Org. Geochem. 30, 1193–1200.
Sun, C.F., Ma, Y.Y., 2015. Effects of non-linear temperature and precipitation trends on Loess Plateau droughts. Quat. Int. 372, 175–179.
Sun, Y.B., Clemens, S.C., Morrill, C., Lin, X.P., Wang, X.L., An, Z.S., 2012. Influence of Atlantic meridional overturning circulation on the East Asian winter monsoon. Nat. Geosci. 5, 46–49.
Sun, Y.B., Kutzbach, J., An, Z.S., Clemens, S.C., Liu, Z.Y., Liu, W.G., Liu, X.D., Shi, Z.G., Zheng, W.P., Liang, L.J., 2015. Astronomical and glacial forcing of East Asian summer monsoon variability. Quat. Sci. Rev. 115, 132–142.
Tang, C.Y., Yang, H., Dang, X.Y., Xie, S.C., 2017. Comparison of paleotemperature reconstructions using microbial tetraether thermometers of the Chinese loess-paleosol sequence for the past 350000 years. Sci. China Earth Sci. 60, 1–12.
Thomas, E.K., Clemens, S.C., Prell, W.L., Herbert, T.D., Huang, Y.S., Liu, Z.Y., Sinninghe Damsté, J.S., Sun, Y.B., Wen, X.Y., 2014. Temperature and leaf wax δ^2H records demonstrate seasonal and regional controls on Asian monsoon proxies. Geology 42, 1075–1078.
Thomas, E.K., Huang, Y.S., Clemens, S.C., Colman, S.M., Morrill, C., Wegener, P., Zhao, J.T., 2016. Changes in dominant moisture sources and the consequences for hydroclimate on the northeastern Tibetan Plateau during the past 32 kyr. Quat. Sci. Rev. 131, 157–167.
Tierney, J.E., deMenocal, P.B., 2013. Abrupt shifts in Horn of Africa hydroclimate since the last glacial maximum. Science 342, 843–846.
Torrence, C., Compo, G.P., 1998. A practical guide to wavelet analysis. Bull. Am. Meteorol. Soc. 79, 61–78.
Wang, Y.J., Cheng, H., Edwards, R.L., Kong, X.G., Shao, X.H., Chen, S.T., Wu, J.Y., Jiang, X.Y., Wang, X.F., An, Z.S., 2008. Millennial-and orbital-scale changes in the East Asian monsoon over the past 224,000 years. Nature 451, 1090–1093.
Wang, Z., Liu, W.G., Liu, Z.H., Wang, H.Y., He, Y.X., Zhang, F., 2013. A 1700-year *n*-alkanes hydrogen isotope record of moisture changes in sediments from Lake Sugan in the Qaidam Basin, northeastern Tibetan Plateau. Holocene 23, 1350–1354.
Waters, C.N., Zalasiewicz, J., Summerhayes, C., Barnosky, A.D., Poirier, C., Gałuszka, A., Cearreta, A., Edgeworth, M., Ellis, E.C., Ellis, M., 2016. The Anthropocene is functionally and stratigraphically distinct from the Holocene. Science 351, aad2622. http://dx.doi.org/10.1126/science.aad2622.
Yan, L.B., 2015. Characteristics of temperature and precipitation on the Loess Plateau from 1961 to 2014. J. Earth Environ. 6, 226–282. http://dx.doi.org/10.7515/JEE201505003.
Yang, H., Pancost, R.D., Dang, X.Y., Zhou, X.Y., Evershed, R.P., Xiao, G.Q., Tang, C.Y., Gao, L., Guo, Z.T., Xie, S.C., 2014. Correlations between microbial tetraether lipids and environmental variables in Chinese soils: optimizing the paleo-reconstructions in semi-arid and arid regions. Geochim. Cosmochim. Acta 126, 49–69.
Yang, S.L., Ding, Z.L., Li, Y.Y., Wang, X., Jiang, W.Y., Huang, X.F., 2015. Warming-induced northwestward migration of the East Asian monsofon rain belt from the Last Glacial Maximum to the mid-Holocene. Proc. Natl. Acad. Sci. U.S.A. 112, 13178–13183. http://dx.doi.org/10.1073/pnas.1504688112.
Yao, Y., Yang, H., Liu, W.G., Li, X.Z., Chen, Y.W., 2015. Hydrological changes of the past 1400 years recorded in δD of sedimentary n-alkanes from Poyang Lake, southeastern China. Holocene 413, 94–99.
Zhou, W.J., Chen, M.B., Kong, X.H., Xian, F., Du, Y.J., Wu, Z.K., Song, S.H., Kang, Z.H., 2015. Mean value concept based "Residual Trace Approach"—application to paleoprecipitation reconstruction over the Chinese Loess Plateau. J. Earth Environ. 6, 382–392. http://dx.doi.org/10.7515/JEE201506002.
Zhou, W.J., Xian, F., Beck, W.J., Jull, A.J.T., An, Z.S., Wu, Z.K., Liu, M., Chen, M.B., Priller, A., Kutschera, W., 2010. Reconstruction of 130-kyr relative geomagnetic intensities from ^{10}Be in two Chinese loess sections. Radiocarbon 52, 129–147.